Structural imaging of native cryo-preserved secondary cell walls reveals the presence of macrofibrils and their formation requires normal cellulose, lignin and xylan biosynthesis.

Jan J. Lyczakowski[1,2,*], Matthieu Bourdon[3], Oliver M. Terrett[1], Ykä Helariutta[3,4], Raymond Wightman[3,] and Paul Dupree[1,2,**]**

[1] Department of Biochemistry, University of Cambridge, Tennis Court Road, Cambridge, CB2 1QW, UK

[2] Natural Material Innovation Centre, University of Cambridge, 1 Scroope Terrace, Cambridge, CB2 1PX, UK

[3] The Sainsbury Laboratory, University of Cambridge, Bateman Street, Cambridge, CB2 1LR, UK

[4] Institute of Biotechnology/Department of Biological and Environmental Sciences, University of Helsinki, FIN-00014, Finland

* Current affiliation: Department of Plant Biotechnology, Faculty of Biochemistry, Biophysics and Biotechnology, Jagiellonian University, Gronostajowa 7, 30-387 Krakow, Poland.

**** Correspondence:**
Address correspondence to Raymond Wightman (raymond.wightman@slcu.cam.ac.uk) or Paul Dupree (pd101@cam.ac.uk).

Keywords: SEM, cell walls, macrofibrils, cellulose, xylan, lignin, softwood, hardwood

Cell wall macrofibrils are composed of cellulose, xylan and lignin

1   Abstract

30

31   The woody secondary cell walls of plants are the largest repository of renewable carbon biopolymers
32   on the planet. These walls are made principally from cellulose and hemicelluloses and are impregnated
33   with lignin. Despite their importance as the main load bearing structure for plant growth, as well as
34   their industrial importance as both a material and energy source, the precise arrangement of these
35   constituents within the cell wall is not yet fully understood. We have adapted low temperature scanning
36   electron microscopy (cryo-SEM) for imaging the nanoscale architecture of angiosperm and
37   gymnosperm cell walls in their native hydrated state. Our work confirms that cell wall macrofibrils,
38   cylindrical structures with a diameter exceeding 10 nm, are a common feature of the native hardwood
39   and softwood samples. We have observed these same structures in *Arabidopsis thaliana* secondary cell
40   walls, enabling macrofibrils to be compared between mutant lines that are perturbed in cellulose,
41   hemicellulose and lignin formation. Our analysis indicates that the macrofibrils in Arabidopsis cell
42   walls are dependent upon the proper biosynthesis, or composed, of cellulose, xylan and lignin. This
43   study establishes that cryo-SEM is a useful additional approach for investigating the native nanoscale
44   architecture and composition of hardwood and softwood secondary cell walls and demonstrates the
45   applicability of Arabidopsis genetic resources to relate fibril structure with wall composition and
46   biosynthesis.

2   Introduction

47

48   The majority of carbon in terrestrial biomass is stored in forests as wood (Ramage et al., 2017, Pan et
49   al., 2011). The current classification system distinguishes two types of timber. Wood from Angiosperm
50   trees is known as hardwood and the wood made by Gymnosperm species is described as softwood
51   (Ramage et al., 2017). Despite significant differences in tissue organisation and chemical composition,
52   both these types of timber are almost entirely formed from plant secondary cell walls – an extracellular
53   matrix made primarily from cellulose, lignin and hemicelluloses (Schweingruber, 2007). Considering
54   the ecological and industrial importance of wood and other cell wall materials, our knowledge of the
55   exact arrangement of these polymers in the cell wall remains poor. A better understanding of the
56   molecular architecture and ultrastructure of cell walls is needed to describe the complex spatio-
57   temporal deposition pattern of the cell wall polymers. This may contribute to the development of more
58   efficient biofuel feedstocks (Loque et al., 2015), to the improvement in our understanding of novel
59   biomaterials such as nanocellulose (Jarvis, 2018), and to applications such as advanced approaches for
60   the use of timber in the construction industry (Ramage et al., 2017)

61   Cellulose is the main constituent of plant cell walls (Pauly and Keegstra, 2008). At the molecular level,
62   cellulose has a simple repeating structure of β-1,4-linked glucopyranosyl residues. These glucan chains
63   coalesce to form a crystalline cellulose microfibril. The exact structure of the microfibril is unknown,
64   however, it has been suggested the elementary microfibril consists of 18 or 24 individual glucan chains
65   (Gonneau et al., 2014, Hill et al., 2014, Turner and Kumar, 2017). Individual cellulose microfibrils
66   associate to form larger order structures known as macrofibrils (Niklas, 2004). In plant primary cell
67   walls this close-contact association may be limited to selected parts of the microfibril which is proposed
68   to lead to formation of so-called biomechanical hotspots (Cosgrove, 2014). A range of imaging and
69   spectroscopic techniques has been used to investigate cellulose macrofibrils in secondary cell walls, as
70   reviewed by (Purbasha et al., 2009), but due to technical challenges the precise structure in native,
71   unprocessed, hydrated secondary cell walls remains poorly described. Lignin is the main non-
72   polysaccharide component of both hardwood and softwood and is made by coupling of monolignol
73   radicals in secondary cell walls. Three main monolignols exist in plants, which, once turned into
74   chemical radicals by the activity of laccases and peroxidases, can couple in a random manner to form

75   a lignin polymer made from guaiacyl (G), syringyl (S), and p-hydroxyphenyl (H) units (Ralph et al.,
76   2004). The monolignol composition of hardwood and softwood differs, with the former consisting of
77   predominantly S and G units and the latter being made almost solely from G units (Vanholme et al.,
78   2010). The process of lignification is important for wood mechanical properties. Arabidopsis mutant
79   plants with reduced lignin content or altered monolignol composition often have collapsed xylem
80   vessels and can be severely dwarfed (Bonawitz and Chapple, 2010). Lignin is proposed to associate
81   with cell wall polysaccharides to form the recalcitrant matrix (Terrett and Dupree, 2019).

82   Xylan and galactoglucomannan are the principal hemicelluloses in hardwood and softwood. Xylan is
83   a polymer of β-1,4-linked xylopyranosyl residues and is the main hemicellulose in hardwood but is
84   also present in softwood (Scheller and Ulvskov, 2010). Hardwood and softwood xylans carry α-1–2
85   linked glucuronic acid (GlcA) branches which can be methylated on carbon 4 leading to formation of
86   4-O-Methyl-glucuronic acid (MeGlcA) (Scheller and Ulvskov, 2010). In addition to GlcA and
87   MeGlcA (together, [Me]GlcA) decorations, hardwood xylan hydroxyls are acetylated on carbon 2,
88   carbon 3 or both carbons of the monomer. The softwood xylan, in addition to the MeGlcA branches,
89   carries α-1,3–linked arabinofuranosyl decorations (Scheller and Ulvskov, 2010, Busse-Wicher et al.,
90   2016b). The presence of [Me]GlcA branches on xylan is important for the maintenance of biomass
91   recalcitrance (Lyczakowski et al., 2017) and, together with acetylation in hardwood and arabinose
92   decorations in softwood, these substitutions are mostly distributed with an even pattern on xylosyl units
93   (Bromley et al., 2013, Busse-Wicher et al., 2014, Busse-Wicher et al., 2016b, Martinez-Abad et al.,
94   2017). This so-called 'compatible' patterning of xylan substitutions is thought to allow the hydrogen
95   bonding between xylan, in a two-fold screw conformation, and the hydrophilic surface of the cellulose
96   microfibril (Busse-Wicher et al., 2016a, Simmons et al., 2016, Grantham et al., 2017).
97   Galactoglucomannan (GGM) is the main hemicellulose in softwood (Scheller and Ulvskov, 2010) but
98   is also present in hardwood xylem. GGM has a backbone formed from both β-1,4-linked mannosyl and
99   glucosyl residues with some mannosyl residues substituted by an α-1,6-linked galactosyl branch. The
100 GGM backbone can also be acetylated. The arrangement of mannose and glucose units in softwood
101 GGM is thought to be random, but a recently described regular structure GGM found in Arabidopsis
102 mucilage was proposed to bind to both the hydrophilic and hydrophobic surface of the cellulose
103 microfibril (Yu et al., 2018). *In vitro* studies using TEM and 1D ^{13}C NMR indicate that a range of
104 branched and unbranched mannan and glucomannan structures can interact with bacterial cellulose
105 (Whitney et al., 1998). Softwood GGM is also proposed to interact with the cellulose microfibril
106 (Terashima et al., 2009) and recent evidence demonstrates that it can form covalent linkages with lignin
107 (Nishimura et al., 2018).

108 Although we now have a better understanding of secondary cell wall composition and the nature of the
109 interactions between its main constituents, a picture of the ultrastructural assembly of wall polymers
110 into a secondary cell wall matrix is not yet complete. Solid state NMR (ssNMR) analysis has been
111 applied extensively to the study of polymer interactions in both primary and secondary walls. This, for
112 example, provided evidence that in dried primary wall samples from Arabidopsis, pectin and
113 xyloglucan may be interacting with the cellulose microfibril (Dick-Perez et al., 2011). Analysis of
114 hydrated secondary cell wall of Arabidopsis with solid state NMR indicated that xylan is likely to
115 interact with the hydrophilic surface of the cellulose microfibril as a two-fold screw (Simmons et al.,
116 2016, Grantham et al., 2017). Recent ssNMR analysis indicates that in dried cell walls of grasses, xylan
117 is likely to interact with lignin (Kang et al., 2019). Despite providing excellent insights into the
118 proximity of different cell wall components ssNMR cannot provide information about the assembly of
119 these constituents into higher order structures. Some insights into this process have been achieved with
120 other techniques. This includes application of vibrational microspectroscopy techniques such as FT-IR
121 and Raman to study the orientation of cellulose and other cell wall components in the matrix, as

122 reviewed by (Gierlinger, 2018). AFM has been applied to the study of cell wall matrix assembly, but
123 the work has been focused on primary cell walls (Cosgrove, 2014) and only recent advances allowed
124 nanoscale resolution imaging of dried spruce secondary cell walls (Casdorff et al., 2017). Moreover,
125 insights into the assembly of cellulose microfibrils in wood walls of conifers (Fernandes et al., 2011)
126 and dicots (Thomas et al., 2014) have been obtained using wide-angle X-ray scattering (WAXS) and
127 small-angle neutron scattering (SANS).

128 In addition to these various approaches, other studies have attempted to use scanning electron
129 microscopy (SEM) to study the structure of plant cell walls. Low temperature SEM (cryo-SEM), in
130 which the sample is rapidly frozen and then maintained cold during imaging, has been used to study
131 the collapse of pine needle tracheid cell walls upon prior dehydration (Cochard et al., 2004) and to
132 visualise the bulging of root hairs in the *kojak* (cellulose synthase-like) mutant (Favery et al., 2001).
133 Additionally, higher magnification cryo-SEM has been used to visualise cell walls of wheat awns
134 (Elbaum et al., 2008). Some awn cell walls exhibit structural differences that are dependent upon the
135 level of hydration and cryo-SEM revealed extensive layering within the wall, however, the technique
136 was not further optimised to investigate individual fibrils. Field emission (FE) SEM techniques were
137 effectively used to study the alignment of cellulose microfibrils in Arabidopsis hypocotyls (Refregier
138 et al., 2004), roots (Himmelspach et al., 2003) and stems (Fujita et al., 2013). FE-SEM has also been
139 applied to investigate wood structure, including observations of microfibril alignment in fixed cell
140 walls of fir tracheids (Abe et al., 1997) and lignin distribution in spruce tracheids (Fromm et al., 2003).
141 Importantly, FE-SEM analysis of dehydrated pine and poplar wood suggests that secondary cell walls
142 of these species contain macrofibrils – cylindrical fibrillar structures with a diameter of up to 60 nm,
143 which presumably comprise of bundles of elementary cellulose microfibrils (Donaldson, 2007).
144 Moreover, the diameter of these macrofibrils was observed to increase with increasing lignification,
145 suggesting that the macrofibrils may be formed from association of lignin and cell wall
146 polysaccharides. This analysis was extended further to wood from Ginkgo where the FE-SEM was
147 combined with density analysis to propose a model of macrofibril formation based on cellulose, GGM,
148 xylan and lignin interaction (Terashima et al., 2009).

149 It has been suggested that some of the treatments used in preparation of the FE-SEM cell wall samples
150 have little impact on the microfibril arrangement and that the technique may provide a true
151 representation of native (unprocessed) cell wall features (Marga et al., 2005). The FE-SEM techniques
152 applied to secondary cell wall samples, however, included additional steps such as (i) fixation and
153 exposure to organic solvents (ii) a thermal treatment that may result in some degree of wall degradation
154 (Fromm et al., 2003) and (iii) a thick coating of heavy metal which may impact upon the resolution
155 (Donaldson, 2007), raising questions about the effect these may have on interpretation of the wall
156 structure. Visualisation of native, hydrated, secondary cell walls with environmental FE-SEM has been
157 challenging and the resolution of obtained images has been low (Donaldson, 2007). We present here a
158 technique for the analysis of native, fully-hydrated, secondary cell wall material from angiosperm and
159 gymnosperm plant species using cryo-SEM. The use of an ultrathin 3 nm platinum film, together with
160 cryo-preservation at high vacuum, enabled us to demonstrate that cell wall macrofibrils are a common
161 feature in all types of native secondary cell wall material analysed. Importantly, we were able to detect
162 the presence of macrofibrils in *Arabidopsis thaliana* vessel secondary cell walls. This allowed us to
163 make use of the readily available cell wall-related genetic resources, revealing Arabidopsis macrofibril
164 diameter to be dependent upon cellulose, xylan and lignin.

165

166 **3   Materials and Methods**

3.1   Plant material

Picea abies, (spruce) one-year old branch was acquired from 30-50cm tall potted plants grown outdoors purchased from Scotsdale (Great Shelford, Cambridgeshire, UK). *Ginkgo biloba*, (Ginkgo) material, consisting of the narrow ends of branches of diameter approximately 3-5 mm was obtained from 15 year old trees trees grown at the Cambridge University Botanic Garden. For both spruce and Ginkgo, samples from two individuals were analysed.

Hybrid aspen (*Populus tremula* x *Populus tremuloides*, clone T89), referred to as poplar in the text, was grown *in vitro* (20°C, with a 16-h light, 8-h dark photoperiod, with illumination at 85 microeinstein.m-2.s-1) during 76 to 80 days after micro-propagation on 1/2MS media with vitamins (Duchefa M0222), 1% sucrose, 0.7% Agar. Samples from three individuals were analysed. For field grown poplar (*Populus tremula*), material was obtained from one year old branches of two approximately 30 year old individuals grown at the Cambridge University Botanic Garden.

Arabidopsis thaliana (Arabidopsis) Columbia-0 ecotype plants were grown in a cabinet maintained at 21 °C, with a 16-h light, 8-h dark photoperiod. Stem material was collected from 7-week-old plants. Mutant insertion lines described in published work were used in this study. Specifically, Col-0 ecotype *irx3-7* plants (Simmons et al., 2016, Kumar and Turner, 2015), representing a mutant allele of CESA7, *irx9-1* (Brown et al., 2005), *irx10-1* (Brown et al., 2005), *esk1-5* (Lefebvre et al., 2011, Grantham et al., 2017), *4cl1-1* (Vanholme et al., 2012), *lac4-2* (Berthet et al., 2011) and *csla2-1csla3-2csla9-1* (Goubet et al., 2009) were studied. Mutants of *IRX1* and *IRX5* gene were in Ler ecotype (Taylor et al., 2003). Plants were analysed alongside the Col-0 or Ler wild type (WT) material. For each genotype three individuals were analysed.

3.2   Cryo-SEM sample preparation and imaging

Fresh stems of 7 week old Arabidopsis plants were prepared for imaging as outlined in Supplementary Material Figure S1. Firstly, 1 cm length sections were cut from the bottom part of the stems and mounted vertically in recessed stubs containing a cryo glue preparation consisting of a 3:1 mixture of Tissue-Tec (Scigen Scientific, USA) and Aquadog colloidal graphite (Agar Scientific, Stansted, UK) (see steps 1 to 4 on Figure S1). Stem sections were immediately (within 5 minutes of harvest) plunge frozen in liquid nitrogen slush (step 5 on Figure S1), transferred under vacuum, fractured and then coated with 3 nm of platinum (step 6 on Figure S1) using a PT3010T cryo-apparatus fitted with a film thickness monitor (Quorum Technologies, Lewes, UK). The short time between freezing and harvesting serves to prevent drying of the sample where only the exposed surface, not the fractured face, is expected to exhibit some water loss during the short time it is exposed to air. Finally, fractured stems were imaged using a Zeiss EVO HD15 Scanning Electron Microscope (step 7 on Figure S1) and maintained at -145 °C using a Quorum cryo-stage assembly. The electron source is a Lanthanum Hexaboride HD filament. Images were acquired using a secondary electron detector and an accelerating voltage of between 5 and 8 kV with a working distance between 4 and 6 mm. Quantification of the width of cell wall macrofibrils was performed using ImageJ software (Schneider et al., 2012). For the measurements of macrofibril width between 25 and 50 macrofibrils were selected at random on each image analysed (Figure 1a). To quantify the width a line was drawn parallel to the fibril axis. The length of a second line, perpendicular to the fibril axis line and across the width of the macrofibril, was quantified as the macrofibril width (Figure 1b). Each fibril width measurement was standardised for the platinum layer applied during the coating process by subtracting the width of the standardised coat from the original measurement. Imaging without the cryo-preservation was performed by visualising hand sectioned platinum coated specimens with the stage maintained at room temperature. For preparation of these samples all freezing steps were omitted.

Cell wall macrofibrils are composed of cellulose, xylan and lignin

212 **3.3   Sampling and statistical analysis**

213 For spruce, Ginkgo and field grown poplar, stem sections were taken from two individual trees and
214 150 macrofibrils were measured from three tracheids/vessels that had each been coated with platinum
215 separately. Imaging of poplar was performed in technical triplicate from three *in vitro* grown trees and
216 150 poplar macrofibrils were measured from three separately coated vessels as for the gymnosperm
217 samples. For Arabidopsis, cryo-SEM imaging of vessels was carried out on three biological replicates,
218 each from separate individuals. 150 macrofibril diameters were measured across the three individuals.

219 Statistical analysis was performed using packages available with R software (Team, 2014). Statistical
220 tests, either Student's T test or ANOVA, used to compare average measurements for samples are
221 defined in Figure legends. The variance between each pairwise combination was estimated to be similar
222 with Levene's test.

223 **4   Results**

224 **4.1   Softwood and hardwood secondary cell walls contain macrofibrils**

225 In order to investigate and compare the nanoscale architecture of gymnosperm and angiosperm cell
226 walls we analysed stem sections taken from spruce, Ginkgo and poplar using cryo-SEM. Stems were
227 placed in the SEM specimen stub and immediately frozen in nitrogen slush, fractured and then coated
228 with platinum, before being passed in to the SEM chamber for imaging. Nitrogen slush is a suspension
229 of solid nitrogen that enables high freezing rates, greatly reducing the Leidenfrost effect during plunge
230 freezing and thus minimising structural damage (Sansinena et al., 2012). The fine grain size attributed
231 to platinum sputtering allows small and densely packed objects to be resolved. This rapid sample
232 preparation protocol serves to better maintain sample hydration levels and native structures for optimal
233 EM imaging in a high vacuum environment.

234 We first investigated whether our cryo-SEM protocol gave comparable results to the previous FE-SEM
235 analysis of both softwood and hardwood secondary cell walls (Donaldson, 2007). To examine if
236 macrofibrils are found in natively hydrated, non-pretreated cell walls, cryo-SEM imaging was
237 performed on unprocessed, frozen softwood and hardwood samples. For observing gymnosperm cell
238 wall architecture, we first prepared softwood samples from spruce and used a low magnification to see
239 an overview of stem cross-section (Figure 2a) and tracheid structure (Figure 2b). The inner part of the
240 stem cross section was composed of densely packed xylem tracheids, each surrounded by cell walls.
241 To investigate the appearance of the secondary cell walls, higher magnification images of these parts
242 of tracheid cells were acquired. This enabled us to observe that the tracheid cell walls contain fibrous
243 structures which frequently assembled into larger aggregates (Figure 2c and 2d, red arrows). After a
244 further increase in magnification, individual fibrils became resolvable (Figure 2e and 2f) and their
245 diameter was found to exceed the 3 nm diameter calculated for a single softwood elementary
246 microfibril (Fernandes et al., 2011). Therefore the observed fibrils, if composed of cellulose, represent
247 a higher order structure that fits the description of a "macrofibril" (Niklas, 2004, Donaldson, 2007).
248 Similarly to spruce stem, sections from another gymnosperm, the Ginkgo, were also observed to
249 contain macrofibrils (Figure S2). These data show that, in line with previously reported SEM imaging
250 of dried, processed plant material (Donaldson, 2007, Terashima et al., 2009), the native, hydrated cell
251 walls of spruce and Ginkgo also contain macrofibrils. Therefore, these structures may contribute to the
252 higher order assembly of native gymnosperm cell walls.

253 We extended the analysis to the model hardwood species, poplar. Vessels, a distinct cell type of
254 hardwood xylem, were clearly visible using low magnification (Figure 3a and 3b). In addition to the

255   vessels, xylem fibre cells were also observed (Figure 3b; red and yellow arrows for vessels and fibre
256   cells respectively). For some cells we were able to observe spiral thickenings which were preserved
257   during sample preparation and extended above the surface of the fracture plane (Figure 3b). We focused
258   upon the vessel cell walls which showed clearly visible fibrous structures at a vessel-to-vessel boundary
259   (Figure 3c). Analysis of vessel cell walls at a higher magnification revealed a clear presence of
260   macrofibril structures, similar to those observed in spruce, in the poplar samples (Figure 3d and 3e).
261   To investigate the dimensions of the macrofibrils we measured their diameter in poplar and spruce
262   (Figure 3f). Our measurements are broadly similar to those reported in a previous study (Donaldson,
263   2007). We carried out comparative analysis of macrofibril diameter between hardwood and softwood
264   by measuring 150 individual macrofibrils in poplar, spruce and Ginkgo. While the diameter of spruce
265   and Ginkgo macrofibrils was not significantly different (Figure S3), the diameter of macrofibrils in
266   poplar secondary cell walls was significantly smaller than that of spruce macrofibrils (Figure 3f).
267   Spruce and Ginkgo were grown in the field while poplar samples were obtained from *in* vitro grown
268   plants. To control for this difference in growth conditions we also analysed samples from field grown
269   poplar trees. There was no statistically significant difference in the macrofibril diameter between the
270   two poplar samples (Figure S4). For both hardwood and softwood we observed variation in the
271   macrofibril diameter. This may reflect biological differences or may be a result of technical challenges
272   associated with macrofibril width measurement.

273   **4.2   Arabidopsis secondary cell walls macrofibrils contain a cellulose scaffold**

274   To further evaluate the nanoscale architecture of plant cell walls and identify possible constituents of
275   the cell wall macrofibrils, the high magnification cryo-SEM imaging was used to analyse wild type
276   (WT) Arabidopsis secondary cell walls (Figure 4). The initial analysis investigated the structure of WT
277   xylem vessels (Figure 4a and 4b). Sets of vessel bundles were detected and, using higher magnification,
278   fibrous structures similar to those observed in spruce and poplar were also visible in the fractured
279   Arabidopsis material. The width of WT Arabidopsis macrofibrils was comparable to that of poplar
280   macrofibrils but not spruce and suggests Arabidopsis macrofibrils could be used as a good structural
281   model for hardwoods (Figure S3, S4). Despite the use of ultra-thin platinum coating, the use of SEM
282   without the cryo-preservation steps did not allow us to observe the Arabidopsis macrofibrils with good
283   resolution (Figure S5) highlighting the critical importance of sample cryo-preservation to resolve a
284   native cell wall ultrastructure.

285   Based on the data available in the literature, we hypothesized that the macrofibrils may be mostly
286   composed of cellulose (Fahlen and Salmen, 2002, Donaldson, 2007). To investigate this, and to
287   understand the nature of these macrofibrils further, we performed a comparative analysis between WT
288   vessel cell walls (Figure 4c) and a commercially available fibrous cellulose standard (Figure 4d)
289   extracted from cotton linters and consisting of 99% pure cellulose (Sczostak, 2009). In this experiment,
290   clear individual fibrils with distinct bright termini were observed in both samples indicating that the
291   vessel wall macrofibrils have a similar appearance to the cellulose fibrils present in this polysaccharide
292   standard. To determine whether these macrofibrils are dependent upon the proper production of
293   cellulose, the morphology of WT Arabidopsis vessel cell walls (Figure 4e and 4g) was compared to
294   that of the *irx3* mutant (Figure 4f and 4h). IRX3 is one of three CESA proteins that make up the
295   secondary wall cellulose synthase complex and *irx3* plants are almost completely devoid of cellulose
296   in their secondary cell walls, but not primary cell walls (Taylor et al., 1999). As previously reported,
297   *irx3* plants had collapsed vessels (Figure S6), since secondary cell wall cellulose contributes to vessel
298   wall strength (Turner & Somerville, 1997). Interestingly, the *irx3* stems lacked the fibrous structures
299   in their vessel secondary cell walls and, in contrast to WT, the *irx3* cell walls were formed from a
300   largely amorphous matrix (Figure 4f). It is likely that this matrix is composed of xylan and lignin,

Cell wall macrofibrils are composed of cellulose, xylan and lignin

301 which can still be deposited in the secondary cell wall in the absence of IRX3 activity (Takenaka et al.,
302 2018). Some structures which may resemble cellulose fibrils were present in the primary cell walls of
303 *irx3* plants (Figure S6). To further support these observations we analysed the cell walls of plants
304 mutated in *IRX1* and *IRX5,* encoding other members of the secondary cell wall cellulose complex
305 (Figure S7). Similar to *irx3,* the *irx1* and *irx5* plants lacked fibril-type structures in their cell walls.
306 Taken together, the data show that macrofibril formation is dependent upon cellulose production.

**4.3   Reduction in cell wall xylan and lignin, but not in galactoglucomannan content decreases
307 the dimensions of Arabidopsis macrofibrils**
308

309 To investigate the role of xylan in macrofibril formation, cryo-SEM was used to visualise the secondary
310 walls from *irx9*, *irx10* and *esk1* Arabidopsis plants (Figure 5a and S8, 5b and S9, 5c and S10). IRX9
311 and IRX10 are required for proper xylan synthesis and mutations in the corresponding genes lead to
312 cell wall weakening and collapse of xylem vessels in the Arabidopsis model (Brown et al., 2007, Bauer
313 et al., 2006, Brown et al., 2005). The *irx9* plants have impaired xylan synthesis resulting in a decrease
314 of xylan by more than 50% compared to WT (Brown et al., 2007). In *irx10* plants the reduction in
315 xylan content is smaller and does not exceed 20% (Brown et al., 2009). Macrofibrils are clearly
316 observed in *irx9* and *irx10* Arabidopsis (Figure 5a and 5b). However, the median macrofibril diameter
317 between WT and *irx9* cell wall fibres showed a ~30% reduction in the xylan synthesis mutant (Figure
318 5g). The median macrofibril diameter of *irx10* plants was ~10% smaller than that of WT Arabidopsis
319 (Figure 5g). Although there was a wide variation in macrofibril diameter within each genotype, the
320 difference between the WT macrofibril diameter and the one quantified for the two mutants is
321 statistically significant, suggesting that xylan is incorporated along with cellulose to generate the
322 normal macrofibril size. To investigate the role of xylan-cellulose interaction in the macrofibril
323 formation we assessed the macrofibril size in the *esk1* Arabidopsis mutant (Figure 5c). Mutation in the
324 *ESK1* gene results in reduction of xylan acetylation, but not in a decrease in xylan quantity (Xiong et
325 al., 2013), which leads to changes in xylan [Me]GlcA patterning and loss of interaction between xylan
326 and the hydrophilic surface of the cellulose microfibril (Grantham et al., 2017). In line with the results
327 observed for *irx9* and *irx10* plants the loss of xylan-cellulose interaction caused a reduction in the
328 macrofibril diameter (Figure 5g).

329 Previous work in softwood suggested that lignin (Donaldson, 2007) and galactoglucomannan (GGM)
330 (Terashima et al., 2009) may be involved in macrofibril formation. To investigate the role of these two
331 cell wall components in the maintenance of macrofibril structure we performed imaging of *4cl1* (Figure
332 5d and S11), *lac4* (Figure 5e and S12) and *csla2/3/9* (Figure 5f and S13) mutant Arabidopsis cell walls.
333 Both 4CL1 and LAC4 are involved in lignin biosynthesis and plants mutated in genes encoding these
334 enzymes have a 30% and 15% reduction in lignin content respectively (Li et al., 2015, Berthet et al.,
335 2011). The median macrofibril diameter for both *4cl1* and *lac4* was significantly smaller than that
336 calculated for WT (Figure 5g). Importantly, the extent of the reduction in macrofibril diameter was in
337 line with the decrease in the lignin content observed for the two mutants, with *4cl1* macrofibrils being
338 ~15% smaller than the WT ones and *lac4* macrofibrils having ~7% reduction in the median diameter.
339 Proteins from the CSLA family are involved in the biosynthesis of a hemicellulose
340 galactoglucomannan and mutations in *csla2/3/9* leads to nearly complete loss of stem GGM in the
341 Arabidopsis model (Goubet et al., 2009). Our quantitative analysis indicates that the diameter of
342 macrofibrils of *csla2/3/9* Arabidopsis was not significantly different to that of the WT plants (Figure
343 5g).

344

8

5   Discussion

The native nanoscale architecture of woody plant secondary cell walls remains poorly understood due to the challenges of keeping the sample hydrated, which is incompatible with some types of techniques. Studies that analyse dehydrated and fixed plant cell wall samples with FE-SEM (Donaldson, 2007), together with other work which includes SANS experiments investigating spruce (Fernandes et al., 2011) and bamboo samples (Thomas et al., 2015), suggest there is a higher order arrangement of cellulose microfibrils in plant secondary cell walls. Our work reports the application of a cryo-SEM based analysis technique which, using exclusively samples that have not been dried, heated or chemically processed, indicates that secondary cell wall cellulose microfibrils are likely to come together to form larger macrofibril structures. Our study strongly suggests that these structures, at least in the model plant species *Arabidopsis thaliana*, are sensitive to changes in xylan and lignin.

Previous studies investigated the presence and diameter of macrofibrils in dehydrated softwood samples (Donaldson, 2007). In line with results presented in our work, Donaldson did observe macrofibrils in cell walls of pine tracheids. Moreover, also in agreement with the results presented here (Figure S4), these softwood macrofibrils were larger than those seen in hardwoods. In softwood, in addition to various patterned types of xylan (Busse-Wicher et al., 2016b, Martinez-Abad et al., 2017), most of which are likely to be compatible with binding to the hydrophilic surface of the cellulose fibril, the cell walls contain large quantities of acetylated GGM (Scheller and Ulvskov, 2010) which may contribute to macrofibril width. Indeed, gymnosperm GGM was proposed to interact with the cellulose microfibril in cell walls of Ginkgo (Terashima et al., 2009). Therefore, the significant difference in macrofibril diameter observed between hardwood and softwood samples may be due to the differences in the cell wall composition. Consequently, we hypothesize that in gymnosperms, GGM, along with xylan, may contribute to the macrofibril size in a way similar to what we observed for xylan in Arabidopsis macrofibrils. With an average diameter ranging between 20 and 34 nm, the size of pine macrofibrils measured by Donaldson was somewhat smaller than that measured in spruce wood in the current work. However, these observations are not necessarily inconsistent. Donaldson dehydrated the wood samples prior to the SEM imaging. As the spacing between bundled softwood cellulose microfibrils, estimated to be equal to 3 nm by small angle neutron scattering, is sensitive to wood hydration levels (Fernandes et al., 2011), at least part of the difference in the macrofibril diameter might be due to the changes in the water content within the sample analysed with SEM. Interestingly, Donaldson reported that macrofibrils in dried poplar wood, depending on their position in cell wall, have an average diameter ranging from 14 to 18 nm, which is similar to what was measured for both poplar and Arabidopsis as a part of our study. This observation suggests that the softwood macrofibril size may be more sensitive to drying than the hardwood one. This in turn suggests that, in addition to compositional disparities, hydration could contribute to the differences in softwood and hardwood macrofibril characteristics. In addition to providing scientific insight, this result highlights that imaging of the cryo-preserved secondary cell walls offers significant advance over the previously used techniques.

Interestingly, similar to a previous report (Donaldson, 2007), we observed that macrofibrils in both hardwood and softwood have a range of diameters. The reasons for this variation in size are not clear. It is possible that the number of individual cellulose microfibrils that come together to form the macrofibril structure in both hardwood and softwood is not constant. This may be regulated by coordinated movement of CesA complexes or their density during cell wall synthesis (Li et al., 2016). It was proposed that the macrofibril diameter is proportional to the degree of cell wall lignification (Donaldson, 2007), which may also vary between the structures. This hypothesis is supported by our results which indicate that the cell wall lignin content influences macrofibril diameter in Arabidopsis.

Cell wall macrofibrils are composed of cellulose, xylan and lignin

391   Variations may also originate from environmental conditions. For example, it was shown that wood
392   density may vary correlatively with climate change (Bouriaud et al., 2005). Although much of this
393   effect is likely to be due to cell size and wall thickness, it can be hypothesized that change in wood
394   density may also originate from compositional changes that impact macrofibril assembly and
395   ultrastructure. It would therefore be relevant to assess macrofibrils of perennial trees with samples
396   spanning several years of growth. We cannot rule out that the width variance may originate from the
397   technical limitations of resolving the macrofibrils by SEM. It will be interesting to see if the emerging
398   He-ion technologies, with an increase in resolution and less dependence upon metal coating, reduce
399   this variance (Joens et al., 2013). The cryo-SEM techniques developed as part of our study offer a
400   significant advantage over the previous investigation (Donaldson, 2007) which applied a thicker coat
401   of chromium (mostly 12 nm) that yield films with coarser grains than the thinner (3 nm) platinum films
402   used in our work. Thus, taking the results described by Donaldson and our technological improvements
403   into consideration, we believe that the variance in the macrofibril width observed in both studies is
404   likely to reflect natural material variation.

405   The prominence of macrofibril structures in Arabidopsis cell walls is a surprising discovery of this
406   study. Previously published results using AFM analysis indicate the presence of some bundled
407   microfibrils in primary cell walls of Arabidopsis but the extent of this bundling is lower than what was
408   observed in primary cell wall samples from other species (Zhang et al., 2016). AFM is not yet
409   technically feasible for analysis of bundling of hydrated secondary cell walls although recent technical
410   advances allowed visualisation of dried spruce wood at a nanometer resolution (Casdorff et al., 2017).
411   The observation of the macrofibrils by cryo-SEM in Arabidopsis allowed us to determine the
412   contribution of cellulose, xylan, lignin and galactoglucomannan to macrofibril formation, thanks to the
413   availability of secondary cell wall related mutants in this model. Macrofibrils were completely absent
414   in vessel cell walls of *irx1*, *irx3 and irx5* plants, which lack secondary cell wall cellulose, indicating
415   that proper cellulose biosynthesis is required for formation and assembly of secondary cell walls
416   polymers into macrofibrils. In addition, we observed that vessel macrofibril diameter is significantly
417   decreased in *irx9, irx10* and *esk1* plants, suggesting that xylan may also participate in the correct
418   assembly of such structures. While in *irx9* and *irx10* reduction in macrofibril diameter may be
419   associated with decrease in the xylan content the ~25% reduction in the median macrofibril diameter
420   observed for *esk1* Arabidopsis is harder to explain. Hardwood xylan is proposed to interact with the
421   hydrophilic surface of the cellulose microfibril as a two-fold screw (Simmons et al., 2016, Busse-
422   Wicher et al., 2016a), and this interaction is facilitated by the even pattern of the [Me]GlcA and acetyl
423   branches on the xylan backbone which is lost in *esk1* plants (Grantham et al., 2017). Therefore, the
424   decrease in macrofibril diameter observed in *esk1* Arabidopsis indicates that xylan-cellulose interaction
425   may have a role in spacing or proper coalescence of microfibrils to form the elementary macrofibril. It
426   is unclear why the macrofibril diameter is reduced in *esk1*, but perhaps fewer elementary fibrils are
427   incorporated into each macrofibril when xylan is not interacting with the hydrophilic surface of the
428   cellulose fibril. This may be different to the effect observed in flax where the absence of xylan may
429   lead to aggregation of glucan chains into larger fibres (Thomas et al., 2013). Such difference may be
430   associated with variations in the stoichiometry of the cellulose synthase complex which were recently
431   reported for angiosperms (Zhang et al., 2018).

432   In addition to implicating xylan in the process of macrofibril formation our results indicate that lignin
433   may contribute to assembly of the structures. As such, our results use genetic assignment to extend
434   previous work which has correlated macrofibril diameter with the degree of wall lignification
435   (Donaldson, 2007). Interestingly, we observed that the macrofibril diameter does not correlate with the
436   cell wall GGM content. This may be associated with low abundance of GGM in angiosperms where
437   the polysaccharide accounts for only up to 5% of the cell wall material (Scheller and Ulvskov, 2010).

438 Alternatively, this result may indicate that in Arabidopsis GGM might be not involved in macrofibril
439 formation. GGM may play a more significant role in the macrofibril assembly in gymnosperms where
440 it accounts for up to 30% of the cell wall material. Importantly, all our conclusions are based on the
441 analysis of native, hydrated, cell wall samples. The assignment of cell wall macrofibril composition,
442 in their native state, would be impossible using techniques such as immunogold due to the pre-
443 treatment steps needed before the antibody labelling.

444 In conclusion, our analysis indicates that Arabidopsis vessel cell walls contain fibrous structures
445 composed of cellulose and likely contain xylan and lignin. These structures are present in both
446 hardwood and softwood and have a diameter larger than a single cellulose microfibril. Therefore, these
447 structures can be described as cell wall macrofibrils. The reduction in macrofibril diameter observed
448 in *esk1* Arabidopsis suggests that the interaction between xylan and the hydrophilic surface of the
449 cellulose microfibril may be involved in the assembly of these structures. Therefore, this xylan-
450 cellulose interaction may be important for the maintenance of plant cell wall ultrastructure and
451 mechanical properties (Simmons et al., 2016). The techniques developed here and the discovery of the
452 ubiquitous presence of macrofibrils in hardwood and softwood in their native state will contribute to a
453 better understanding of cell wall assembly processes. Furthermore, the ability to resolve macrofibrils
454 in Arabidopsis, along with the availability of genetic resources in this model, will offer the community
455 a valuable tool to further study the complex deposition of secondary cell walls polymers and their role
456 in defining the cell wall ultrastructure. The assembly of cell wall macrofibrils is likely to influence the
457 properties of wood, such as density, which may vary due to different stimuli such as tree fertilisation
458 (Makinen et al., 2002) or environmental changes (Bouriaud et al., 2005). Therefore, we expect that the
459 methodology described here will enable to correlate the native nanoscale features of the cell walls,
460 such as the macrofibril diameter, or a specific macrofibril patterning within the cell wall, with wood
461 properties. Consequently, our approach may be useful to assess this aspect of wood quality at a new
462 level and could benefit numerous industries ranging from building construction, paper manufacturing
463 and biofuel production to generation of novel biomaterials such as nanocrystalline cellulose.

464

6   Conflict of Interest

466 The authors declare that the research was conducted in the absence of any commercial or financial
467 relationships that could be construed as a potential conflict of interest.

7   Author Contributions

469 JJL designed the study, conducted the experiments, analysed the data and wrote the paper. MB
470 performed poplar imaging experiments, analysed the data and wrote the paper. OMT analysed the data
471 and wrote the paper. YH contributed to data analysis and manuscript preparation, RW designed the
472 study, conducted experiments, analysed the data and wrote the paper. PD designed the study and
473 contributed to data analysis and manuscript preparation.

8   Funding

491 **9   Acknowledgments**

496 **10   List of abbreviations**

497 1D – one dimensional

498 AFM – atomic force microscopy

499 CesA – Cellulose synthase

500 cryo-SEM – low temperature scanning electron microscopy

501 FE-SEM – field emission scanning electron microscopy

502 FT-IR - Fourier-transform infrared spectroscopy

503 GGM – galactoglucomannan

504 He-ion – Helium ion

505 IRX – irregular xylem

506 [Me]GlcA – methylated and unmethylated form of glucuronic acid

507 NMR – nuclear magnetic resonance

508 SANS – small angle neutron scattering

509 TEM – transmission electron microscopy

510 WAXS – wide angle x-ray scattering

511 **11   Data Availability Statement**

512 All quantitative datasets generated and analysed for this study are presented on graphs included in the
513 manuscript and the supplementary files.

514 **12   References**

515 ABE, H., FUNADA, R., OHTANI, J. & FUKAZAWA, K. 1997. Changes in the arrangement of
516   cellulose microfibrils associated with the cessation of cell expansion in tracheids. *Trees-*
517   *Structure and Function,* 11**,** 328-332.
518 BAUER, S., VASU, P., PERSSON, S., MORT, A. J. & SOMERVILLE, C. R. 2006. Development
519   and application of a suite of polysaccharide-degrading enzymes for analyzing plant cell walls.
520   *Proceedings of the National Academy of Sciences of the United States of America,* 103**,**
521   11417-11422.
522 BERTHET, S., DEMONT-CAULET, N., POLLET, B., BIDZINSKI, P., CEZARD, L., LE BRIS, P.,
523   BORREGA, N., HERVE, J., BLONDET, E., BALZERGUE, S., LAPIERRE, C. &
524   JOUANIN, L. 2011. Disruption of LACCASE4 and 17 Results in Tissue-Specific Alterations
525   to Lignification of Arabidopsis thaliana Stems. *Plant Cell,* 23**,** 1124-1137.
526 BONAWITZ, N. D. & CHAPPLE, C. 2010. The Genetics of Lignin Biosynthesis: Connecting
527   Genotype to Phenotype. *Annual Review of Genetics, Vol 44,* 44**,** 337-363.
528 BOURIAUD, O., LEBAN, J. M., BERT, D. & DELEUZE, C. 2005. Intra-annual variations in
529   climate influence growth and wood density of Norway spruce. *Tree Physiology,* 25**,** 651-660.
530 BROMLEY, J. R., BUSSE-WICHER, M., TRYFONA, T., MORTIMER, J. C., ZHANG, Z.,
531   BROWN, D. M. & DUPREE, P. 2013. GUX1 and GUX2 glucuronyltransferases decorate
532   distinct domains of glucuronoxylan with different substitution patterns. *Plant Journal,* 74**,**
533   423-434.
534 BROWN, D. M., GOUBET, F., VICKY, W. W. A., GOODACRE, R., STEPHENS, E., DUPREE, P.
535   & TURNER, S. R. 2007. Comparison of five xylan synthesis mutants reveals new insight into
536   the mechanisms of xylan synthesis. *Plant Journal,* 52**,** 1154-1168.
537 BROWN, D. M., ZEEF, L. A. H., ELLIS, J., GOODACRE, R. & TURNER, S. R. 2005.
538   Identification of novel genes in Arabidopsis involved in secondary cell wall formation using
539   expression profiling and reverse genetics. *Plant Cell,* 17**,** 2281-2295.
540 BROWN, D. M., ZHANG, Z., STEPHENS, E., DUPREE, P. & TURNER, S. R. 2009.
541   Characterisation of IRX10 and IRX10-like reveals an essential role in glucuronoxylan
542   biosynthesis in Arabidopsis. *The Plant Journal,* 57, 732-746.
543 BUSSE-WICHER, M., GOMES, T. C. F., TRYFONA, T., NIKOLOVSKI, N., STOTT, K.,
544   GRANTHAM, N. J., BOLAM, D. N., SKAF, M. S. & DUPREE, P. 2014. The pattern of
545   xylan acetylation suggests xylan may interact with cellulose microfibrils as a twofold helical
546   screw in the secondary plant cell wall of Arabidopsis thaliana. *Plant Journal,* 79**,** 492-506.
547 BUSSE-WICHER, M., GRANTHAM, N. J., LYCZAKOWSKI, J. J., NIKOLOVSKI, N. &
548   DUPREE, P. 2016a. Xylan decoration patterns and the plant secondary cell wall molecular
549   architecture. *Biochemical Society Transactions,* 44**,** 74-78.
550 BUSSE-WICHER, M., LI, A., SILVEIRA, R. L., PEREIRA, C. S., TRYFONA, T., GOMES, T. C.
551   F., SKAF, M. S. & DUPREE, P. 2016b. Evolution of Xylan Substitution Patterns in
552   Gymnosperms and Angiosperms: Implications for Xylan Interaction with Cellulose. *Plant*
553   *Physiology,* 171**,** 2418-2431.
554 CASDORFF, K., KEPLINGER, T., BURGERT, I. 2017. Nono-mechanical characterisation of the
555   wood cell wall by AFM studies: comparison between AC- and QI^{TM} mode. *Plant Methods,*
556   13, 60**.**
557 COCHARD, H., FROUX, F., MAYR, F. F. S. & COUTAND, C. 2004. Xylem wall collapse in
558   water-stressed pine needles. *Plant Physiology,* 134**,** 401-408.

559   COSGROVE, D. J. 2014. Re-constructing our models of cellulose and primary cell wall assembly.
560   *Current Opinion in Plant Biology,* 22, 121-131.
561   DICK-PEREZ, M., ZHANG, Y. A., HAYES, J., SALAZAR, A., ZABOTINA, O. A., HONG, M.
562   2011. Structure and interactions of plant cell-wall polysaccharides by two- and three-
563   dimensional magic-angle-spinning solid-state NMR. *Biochemistry,* 50, 989-1000.
564   DONALDSON, L. 2007. Cellulose microfibril aggregates and their size variation with cell wall type.
565   *Wood Science and Technology,* 41**,** 443-460.
566   ELBAUM, R., GORB, S., FRATZL, P. 2008. Structures in the cell wall that enable hygroscopic
567   movement of wheat awns. *Journal of Structural Biology,* 164, 101-107.
568   FAHLEN, J. & SALMEN, L. 2002. On the Lamellar Structure of the Tracheid Cell Wall. *Plant
569   Biology,* 4, 339-345.
570   FAVERY, B., RYAN, E., FOREMAN, J., LINSTEAD, P., BOUDONCK, K., STEER, M., SHAW,
571   P. & DOLAN, L. 2001. KOJAK encodes a cellulose synthase-like protein required for root
572   hair cell morphogenesis in Arabidopsis. *Genes & Development,* 15**,** 79-89.
573   FERNANDES, A. N., THOMAS, L. H., ALTANER, C. M., CALLOW, P., FORSYTH, V. T.,
574   APPERLEY, D. C., KENNEDY, C. J. & JARVIS, M. C. 2011. Nanostructure of cellulose
575   microfibrils in spruce wood. *Proceedings of the National Academy of Sciences of the United
576   States of America,* 108**,** E1195-E1203.
577   FROMM, J., ROCKEL, B., LAUTNER, S., WINDEISEN, E. & WANNER, G. 2003. Lignin
578   distribution in wood cell walls determined by TEM and backscattered SEM techniques.
579   *Journal of Structural Biology,* 143**,** 77-84.
580   FUJITA, M., HIMMELSPACH, R., WARD, J., WHITTINGTON, A., HASENBEIN, N., LIU, C.,
581   TRUONG, T. T., GALWAY, M. E., MANSFIELD, S. D., HOCART, C. H. &
582   WASTENEYS, G. O. 2013. The anisotropy1 D604N Mutation in the Arabidopsis Cellulose
583   Synthase1 Catalytic Domain Reduces Cell Wall Crystallinity and the Velocity of Cellulose
584   Synthase Complexes. *Plant Physiology,* 162**,** 74-85.
585   GIERLINGER, N. 2018. New insights into plant cell walls by vibrational microspectroscopy.
586   *Applied Spectroscopy Reviews,* 53, 517-551.
587   GONNEAU, M., DESPREZ, T., GUILLOT, A., VERNHETTES, S. & HOFTE, H. 2014. Catalytic
588   Subunit Stoichiometry within the Cellulose Synthase Complex. *Plant Physiology,* 166**,** 1709-
589   1712.
590   GOUBET, F., BARTON, C. J., MORTIMER, J. C., YU, X. L., ZHANG, Z. N., MILES, G. P.,
591   RICHENS, J., LIEPMAN, A. H., SEFFEN, K. & DUPREE, P. 2009. Cell wall glucomannan
592   in Arabidopsis is synthesised by CSLA glycosyltransferases, and influences the progression
593   of embryogenesis. *Plant Journal,* 60**,** 527-538.
594   GRANTHAM, N. J., WURMAN-RODRICH, J., TERRETT, O. M., LYCZAKOWSKI, J. J.,
595   STOTT, K., IUGA, D., SIMMONS, T. J., DURAND-TARDIF, M., BROWN, S. P.,
596   DUPREE, R., BUSSE-WICHER, M. & DUPREE, P. 2017. An even pattern of xylan
597   substitution is critical for interaction with cellulose in plant cell walls. *Nature Plants,* 3**,** 859-
598   865.
599   HILL, J. L., HAMMUDI, M. B. & TIEN, M. 2014. The Arabidopsis Cellulose Synthase Complex: A
600   Proposed Hexamer of CESA Trimers in an Equimolar Stoichiometry. *Plant Cell,* 26**,** 4834-
601   4842.
602   HIMMELSPACH, R., WILLIAMSON, R. E. & WASTENEYS, G. O. 2003. Cellulose microfibril
603   alignment recovers from DCB-induced disruption despite microtubule disorganization. *Plant
604   Journal,* 36**,** 565-575.
605   JARVIS, M. C. 2018. Structure of native cellulose microfibrils, the starting point for nanocellulose
606   manufacture. *Philosophical transactions. Series A, Mathematical, physical, and engineering
607   sciences,* 376.

608 JOENS, M. S., HUYNH, C., KASUBOSKI, J. M., FERRANTI, D., SIGAL, Y. J., ZEITVOGEL, F.,
609   OBST, M., BURKHARDT, C. J., CURRAN, K. P., CHALASANI, S. H., STERN, L. A.,
610   GOETZE, B. & FITZPATRICK, J. A. J. 2013. Helium Ion Microscopy (HIM) for the
611   imaging of biological samples at sub-nanometer resolution. *Scientific Reports,* 3.
612 KANG, X., KIRUI, A., DICKWELLA WIDANAGE, M. C., MENTINK-VIGIER, F., COSGROVE,
613   D. J., WANG, T. 2019. Lignin-polysaccharide interactions in plant secondary cell walls
614   revealed by solid-state NMR. *Nature Communications,* 10, 347.
615 KUMAR, M. & TURNER, S. 2015. Protocol: a medium-throughput method for determination of
616   cellulose content from single stem pieces of Arabidopsis thaliana. *Plant Methods,* 11.
617 LEFEBVRE, V., FORTABAT, M. N., DUCAMP, A., NORTH, H. M., MAIA-GRONDARD, A.,
618   TROUVERIE, J., BOURSIAC, Y., MOUILLE, G. & DURAND-TARDIF, M. 2011.
619   ESKIMO1 Disruption in Arabidopsis Alters Vascular Tissue and Impairs Water Transport.
620   *Plos One,* 6.
621 LI, S. D., BASHLINE, L., ZHENG, Y. Z., XIN, X. R., HUANG, S. X., KONG, Z. S., KIM, S. H.,
622   COSGROVE, D. J. & GU, Y. 2016. Cellulose synthase complexes act in a concerted fashion
623   to synthesize highly aggregated cellulose in secondary cell walls of plants. *Proceedings of the*
624   *National Academy of Sciences of the United States of America,* 113**,** 11348-11353.
625 LI, Y., KIM, J. I., PYSH, L. & CHAPPLE, C. 2015. Four Isoforms of Arabidopsis 4-Coumarate:
626   CoA Ligase Have Overlapping yet Distinct Roles in Phenylpropanoid Metabolism. *Plant*
627   *Physiology,* 169**,** 2409-2421.
628 LOQUE, D., SCHELLER, H. V. & PAULY, M. 2015. Engineering of plant cell walls for enhanced
629   biofuel production. *Current Opinion in Plant Biology,* 25**,** 151-161.
630 LYCZAKOWSKI, J. J., WICHER, K. B., TERRETT, O. M., FARIA-BLANC, N., YU, X. L.,
631   BROWN, D., KROGH, K., DUPREE, P. & BUSSE-WICHER, M. 2017. Removal of
632   glucuronic acid from xylan is a strategy to improve the conversion of plant biomass to sugars
633   for bioenergy. *Biotechnology for Biofuels,* 10.
634 MAKINEN, H., SARANPAA, P. & LINDER, S. 2002. Wood-density variation of Norway spruce in
635   relation to nutrient optimization and fibre dimensions. *Canadian Journal of Forest Research-*
636   *Revue Canadienne De Recherche Forestiere,* 32**,** 185-194.
637 MARGA, F., GRANDBOIS, M., COSGROVE, D. J. & BASKIN, T. I. 2005. Cell wall extension
638   results in the coordinate separation of parallel microfibrils: evidence from scanning electron
639   microscopy and atomic force microscopy. *Plant Journal,* 43**,** 181-190.
640 MARTINEZ-ABAD, A., BERGLUND, J., TORIZ, G., GATENHOLM, P., HENRIKSSON, G.,
641   LINDSTROM, M., WOHLERT, J. & VILAPLANA, F. 2017. Regular Motifs in Xylan
642   Modulate Molecular Flexibility and Interactions with Cellulose Surfaces. *Plant Physiology,*
643   175**,** 1579-1592.
644 NIKLAS, K. 2004. The cell walls that bind the tree of life. *BioScience,* 54, 831-841.
645 NISHIMURA, H., KAMIYA, A., NAGATA, T., KATAHIRA, M. & WATANABE, T. 2018. Direct
646   evidence for alpha ether linkage between lignin and carbohydrates in wood cell walls.
647   *Scientific Reports,* 8.
648 PAN, Y. D., BIRDSEY, R. A., FANG, J. Y., HOUGHTON, R., KAUPPI, P. E., KURZ, W. A.,
649   PHILLIPS, O. L., SHVIDENKO, A., LEWIS, S. L., CANADELL, J. G., CIAIS, P.,
650   JACKSON, R. B., PACALA, S. W., MCGUIRE, A. D., PIAO, S. L., RAUTIAINEN, A.,
651   SITCH, S. & HAYES, D. 2011. A Large and Persistent Carbon Sink in the World's Forests.
652   *Science,* 333**,** 988-993.
653 PAULY, M. & KEEGSTRA, K. 2008. Cell-wall carbohydrates and their modification as a resource
654   for biofuels. *Plant Journal,* 54**,** 559-568.

655 PURBASHA, S., BOSNEAGA, E. AUER, M. 2009. Plant cell walls throughout evolution: towards a
656   molecular understanding of their design principles. *Journal of Experimental Botany,* 60,
657   3615-3635.
658 RALPH, J., LUNDQUIST, K., BRUNOW, G., LU, F., KIM, H., SCHATZ, P. F., MARITA, J. M.,
659   HATFIELD, R. D., RALPH, S. A., CHRISTENSEN, J. H., BOERJAN, W. 2004. Lignins:
660   natural polymers from oxidative coupling of 4-hydroxyphenyl- propanoids. *Phytochemistry*
661   *Reviews,* 3, 29-60.
662 RAMAGE, M. H., BURRIDGE, H., BUSSE-WICHER, M., FEREDAY, G., REYNOLDS, T.,
663   SHAH, D. U., WU, G. L., YU, L., FLEMING, P., DENSLEY-TINGLEY, D., ALLWOOD,
664   J., DUPREE, P., LINDEN, P. F. & SCHERMAN, O. 2017. The wood from the trees: The use
665   of timber in construction. *Renewable & Sustainable Energy Reviews,* 68**,** 333-359.
666 REFREGIER, G., PELLETIER, S., JAILLARD, D. & HOFTE, H. 2004. Interaction between wall
667   deposition and cell elongation in dark-grown hypocotyl cells in Arabidopsis. *Plant*
668   *Physiology,* 135**,** 959-968.
669 SANSINENA, M., SANTOS, M. V., ZARITZKY, N., CHIRIFE, J. 2012. Comparison of heat
670   transfer in liquid and slush nitrogen by numerical simulation of cooling rates for French
671   straws used for sperm cryopreservation. *Theriogenology,* 77, 1717-1721.
672 SCHELLER, H. V. & ULVSKOV, P. 2010. Hemicelluloses. *Annual Review of Plant Biology, Vol*
673   *61,* 61**,** 263-289.
674 SCHNEIDER, C. A., RASBAND, W. S. & ELICEIRI, K. W. 2012. NIH Image to ImageJ: 25 years
675   of image analysis. *Nature Methods,* 9**,** 671-675.
676 SCHWEINGRUBER, F. H. 2007. *Wood structure and environment,* Berlin, Springer.
677 SCZOSTAK, A. 2009. Cotton Linters: An Alternative Cellulosic Raw Material. *Macromolecular*
678   *Symposia,* 280**,** 45-53.
679 SIMMONS, T. J., MORTIMER, J. C., BERNARDINELLI, O. D., POPPLER, A. C., BROWN, S. P.,
680   DEAZEVEDO, E. R., DUPREE, R. & DUPREE, P. 2016. Folding of xylan onto cellulose
681   fibrils in plant cell walls revealed by solid-state NMR. *Nature Communications,* 7.
682 TAKENAKA, Y., WATANABE, Y., SCHUETZ, M., UNDA, F., HILL, J., PHOOKAEW, P.,
683   YONEDA, A., MANSFIELD, S. D., SAMUELS, L., OHTANI, M & DEMURA, T. 2018.
684   Patterned deposition of xylan and lignin is independent from that of the secondary wall
685   cellulose of Arabidopsis xylem vessels. *Plant Cell,* 30, 2663-2676.
686 TAYLOR, N. G., HOWELLS, R. M., HUTTLY, A. K., VICKERS, K. & TURNER, S. R. 2003.
687   Interactions among three distinct CesA proteins essential for cellulose synthesis. *Proceedings*
688   *of the National Academy of Sciences of the United States of America,* 100, 1450-1455.
689 TAYLOR, N. G., SCHEIBLE, W. R., CUTLER, S., SOMERVILLE, C. R. & TURNER, S. R. 1999.
690   The irregular xylem3 locus of arabidopsis encodes a cellulose synthase required for secondary
691   cell wall synthesis. *Plant Cell,* 11**,** 769-779.
692 TEAM, R. C. 2014. *R: A language and environment for statistical computing.* [Online]. Vienna
693   Austria. Available: http://www.R-project.org/ [Accessed].
694 TERASHIMA, N., KITANO, K., KOJIMA, M., YOSHIDA, M., YAMAMOTO, H. &
695   WESTERMARK, U. 2009. Nanostructural assembly of cellulose, hemicellulose, and lignin in
696   the middle layer of secondary wall of ginkgo tracheid. *Journal of Wood Science,* 55**,** 409-416.
697 TERRETT, O. M., DUPREE, P. 2019. Covalent interactions between lignin and hemicelluloses in
698   plant secondary cell walls. *Current Opinion in Biotechnology,* 56, 97-104.
699 THOMAS, L. H., ALTANER, C. M. & JARVIS, M. C. 2013. Identifying multiple forms of lateral
700   disorder in cellulose fibres. *Journal of Applied Crystallography,* 46**,** 972-979.
701 THOMAS, L. H., FORSYTH, V. T., MARTEL, A., GRILLO, I., ALTANER, C. M. & JARVIS, M.
702   C. 2014. Structure and spacing of cellulose microfibrils in woody cell walls of dicots.
703   *Cellulose,* 21, 3887-3895.

704 THOMAS, L. H., FORSYTH, V. T., MARTEL, A., GRILLO, I., ALTANER, C. M. & JARVIS, M.
705   C. 2015. Diffraction evidence for the structure of cellulose microfibrils in bamboo, a model
706   for grass and cereal celluloses. *Bmc Plant Biology,* 15.
707 TURNER, S. & KUMAR, M. 2017. Cellulose synthase complex organization and cellulose
708   microfibril structure. *Philosophical Transactions of the Royal Society A,* 376.
709 TURNER, S. R. & SOMERVILLE, C. R. 1997. Collapsed xylem phenotype of Arabidopsis identifies
710   mutants deficient in cellulose deposition in the secondary cell wall. *Plant Cell,* 9, 689-701.
711 VANHOLME, R., DEMEDTS, B., MORREEL, K., RALPH, J., BOERJAN, W. 2010. Lignin
712   biosynthesis and structure. *Plant Physiology,* 132, 1781-1789.
713 VANHOLME, R., STORME, V., VANHOLME, B., SUNDIN, L., CHRISTENSEN, J. H.,
714   GOEMINNE, G., HALPIN, C., ROHDE, A., MORREEL, K. & BOERJAN, W. 2012. A
715   Systems Biology View of Responses to Lignin Biosynthesis Perturbations in Arabidopsis.
716   *Plant Cell,* 24**,** 3506-3529.
717 WHITNEY, S. E. C., BRIGHAM, J. E., DARKE, A. H., REID, J. S. G. & GIDLEY, M. J. 1998.
718   Structural aspects of the interaction of mannan-based polysaccharides with bacterial cellulose.
719   *Carbohydrate Research,* 307**,** 299-309.
720 XIONG, G., CHENG, K. & PAULY, M. Xylan O-Acetylation Impacts Xylem Development and
721   Enzymatic Recalcitrance as Indicated by the Arabidopsis Mutant tbl29. *Molecular Plant,* 6,
722   1373-1375.
723 YU, L., LYCZAKOWSKI, J. J., PEREIRA, C. S., KOTAKE, T., YU, X., LI, A., MOGELSVANG,
724   S., SKAF, M. S. & DUPREE, P. 2018. The patterned structure of galactoglucomannan
725   suggests it may bind to cellulose in seed mucilage. *Plant Physiology,* 178, 1011-1026.
726 ZHANG, T., ZHENG, Y. Z. & COSGROVE, D. J. 2016. Spatial organization of cellulose
727   microfibrils and matrix polysaccharides in primary plant cell walls as imaged by multichannel
728   atomic force microscopy. *Plant Journal,* 85**,** 179-192.
729 ZHANG, X. Y., DOMINGUEZ, P. G., KUMAR, M., BYGDELL, J., MIROSHNICHENKO, S.,
730   SUNDBERG, B., WINGSLE, G. & NIITTYLA, T. 2018. Cellulose Synthase Stoichiometry
731   in Aspen Differs from Arabidopsis and Norway Spruce. *Plant Physiology,* 177**,** 1096-1107.

732

733 **13   Short legends for supporting material figures:**

734 Figure S1: Overview of the cryo-SEM procedure.

735 Figure S2: Cryo-SEM analysis of Ginkgo cell walls.

736 Figure S3: Comparison of macrofibril diameter in Arabidopsis, poplar, spruce and Ginkgo.

737 Figure S4: Imaging of macrofibrils in field grown poplar.

738 Figure S5: Analysis of native Arabidopsis samples without the cryo-preservation protocol.

739 Figure S6: Cryo-SEM analysis of vessel collapse and primary cell wall cellulose in *irx3* Arabidopsis
740 plants.

741 Figure S7: Analysis of *irx1* and *irx5* cell walls.

742 Figure S8: Further images of *irx9* plants.

743   Figure S9: Further images of *irx10* plants.

744   Figure S10: Further images of *esk1* plants.

745   Figure S11: Further images of *4cl1* plants.

746   Figure S12: Further images of *lac4* plants.

747   Figure S13: Further images of *csla2/3/9* plants.

748

749   **14   Main text figure legends**

750   **Figure 1. Measurement of cell wall macrofibrils. (a)** Example of macrofibrils which would be
751   considered for measurement. Only macrofibrils that were resolvable from their neighbours were
752   analysed. The diameter was measured at a site along the length of the macrofibril and not at the
753   fractured ends. Measurement **(b)** was carried out by placing one line in parallel to the macrofibril and
754   measuring the length of a line perpendicular to it and spanning the width of the structure to be analysed.

755   **Figure 2. cryo-SEM analysis of spruce stem sections. (a)** to **(f)** Representative images of stem
756   sections of one-year-old spruce branch at different magnifications. Red arrows indicate tracheids **(b)**,
757   macrofibril bundles **(c** and **d)** and individual macrofibrils **(e** and **f)**. Scale bars are provided for each
758   image.

759   **Figure 3. cryo-SEM analysis of poplar stem sections (a)** to **(e)** Representative images of stem
760   sections of *in vitro* grown poplar trees at different magnifications. Red arrows show vessels **(b)** and
761   macrofibrils **(c** and **e)**. Yellow arrows indicate fibre cells **(b)**. Higher magnification images **(c, d** and
762   **e)** are presented for vessels. Scale bars are provided for each image. **(f)** Diameter of spruce tracheid
763   cell wall fibrils compared to these observed in poplar vessel cell walls. For each bar 150 individual
764   fibrils were measured. Boxplots mark the median and show between 25th and 75th percentile of the
765   data. *** denotes $p \leq 0.00001$ in Student's t-test.

766   **Figure 4. Analysis of Arabidopsis stem sections and fibrous cellulose. (a)** to **(c)** Imaging of WT
767   vessels at increasing magnification **(d)** Imaging of fibrous cellulose standard from cotton linters shows
768   cell wall fibrils with an appearance similar to structures seen *in planta*. **(e)** Imaging of individual
769   vessels in WT plants. **(f)** Imaging of individual vessels in *irx3* plants. **(g)** and **(f)** Macrofibrils are
770   detectable in WT Arabidopsis and are absent in *irx3* secondary cell walls. Red arrows indicate the
771   macrofibril structures throughout the figure. Scale bars are provided for each image.

772   **Figure 5. Analysis of macrofibrils in mutant Arabidopsis plants.** Representative image of **(a)** *irx9*,
773   **(b)** *irx10*, **(c)** *esk1*, **(d)** *4cl1*, **(e)** *lac4* and **(f)** *csla2/3/9* Arabidopsis macrofibrils. Scale bar corresponds
774   to 200 nm on each image. Red arrows show macrofibrils **(g)** Quantification of macrofibril diameter in
775   WT and mutant Arabidopsis plants. N = 150. Boxplots mark a median and show between 25th and 75th
776   percentile of the data. *** denotes $p \leq 0.00001$, ** denotes $p \leq 0.0001$, * denotes $p \leq 0.05$ in Tukey
777   test following ANOVA when compared to WT, ns indicates lack of statistically significant difference.
778   Additional images of each genotype are shown in figures S8 - S13.

779

(a)

200 nm

(b)

reference line

measurement line

90° angle

250 nm
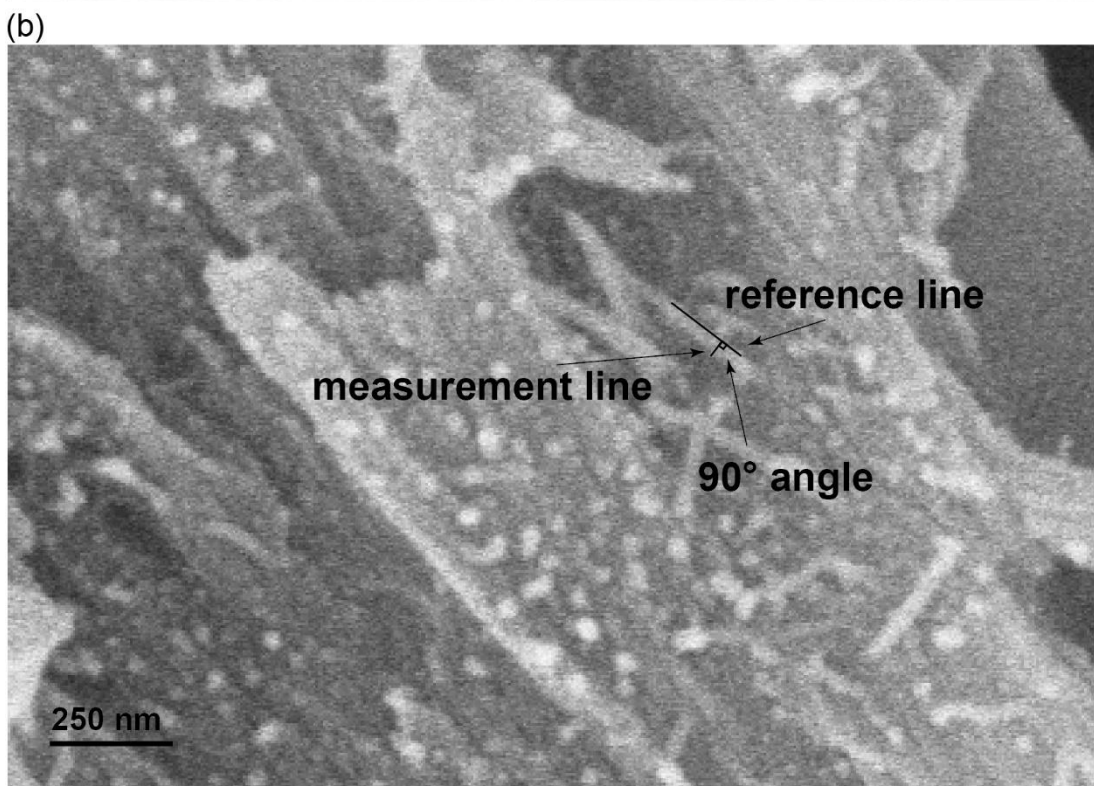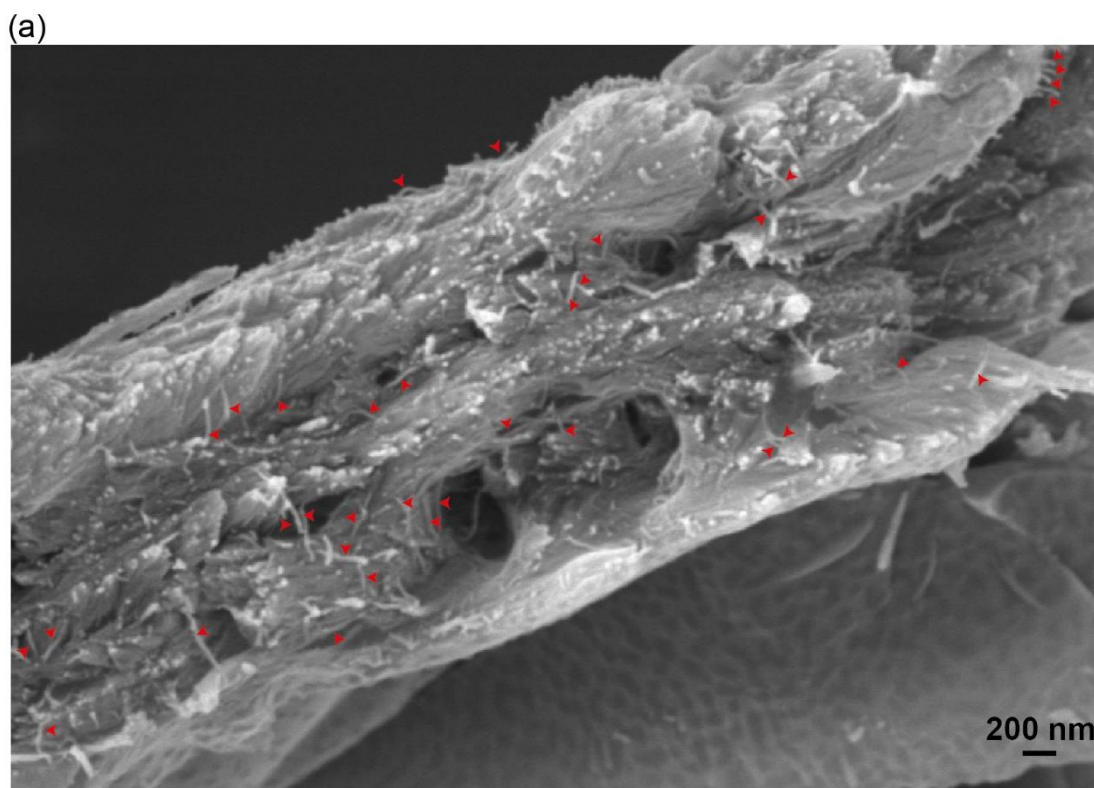
780

781   Figure 1

782

783

Cell wall macrofibrils are composed of cellulose, xylan and lignin
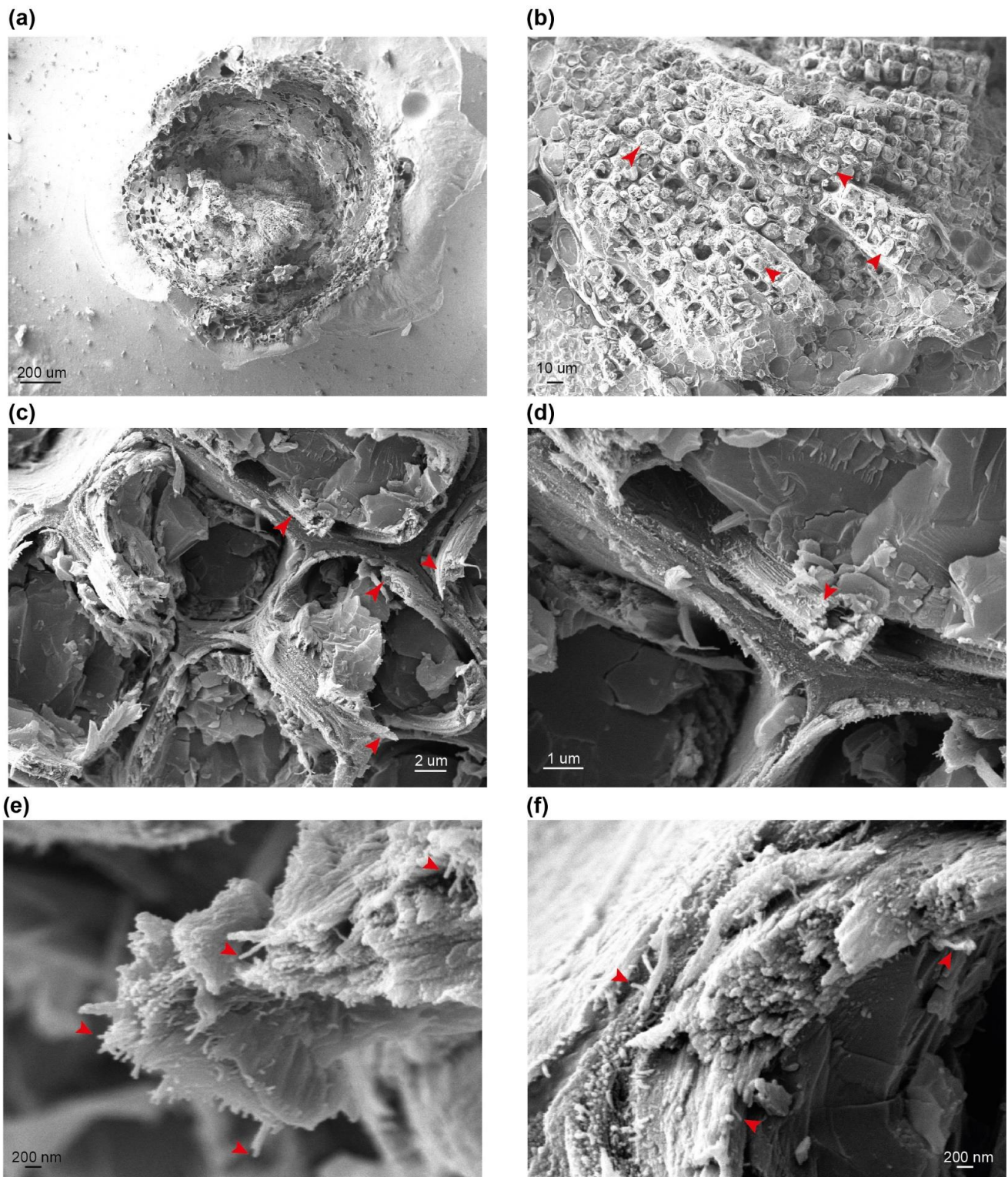
784

785   Figure 2

786

787

788

20

(a)

(b)

(c)

(d)

(e)

(f)

789
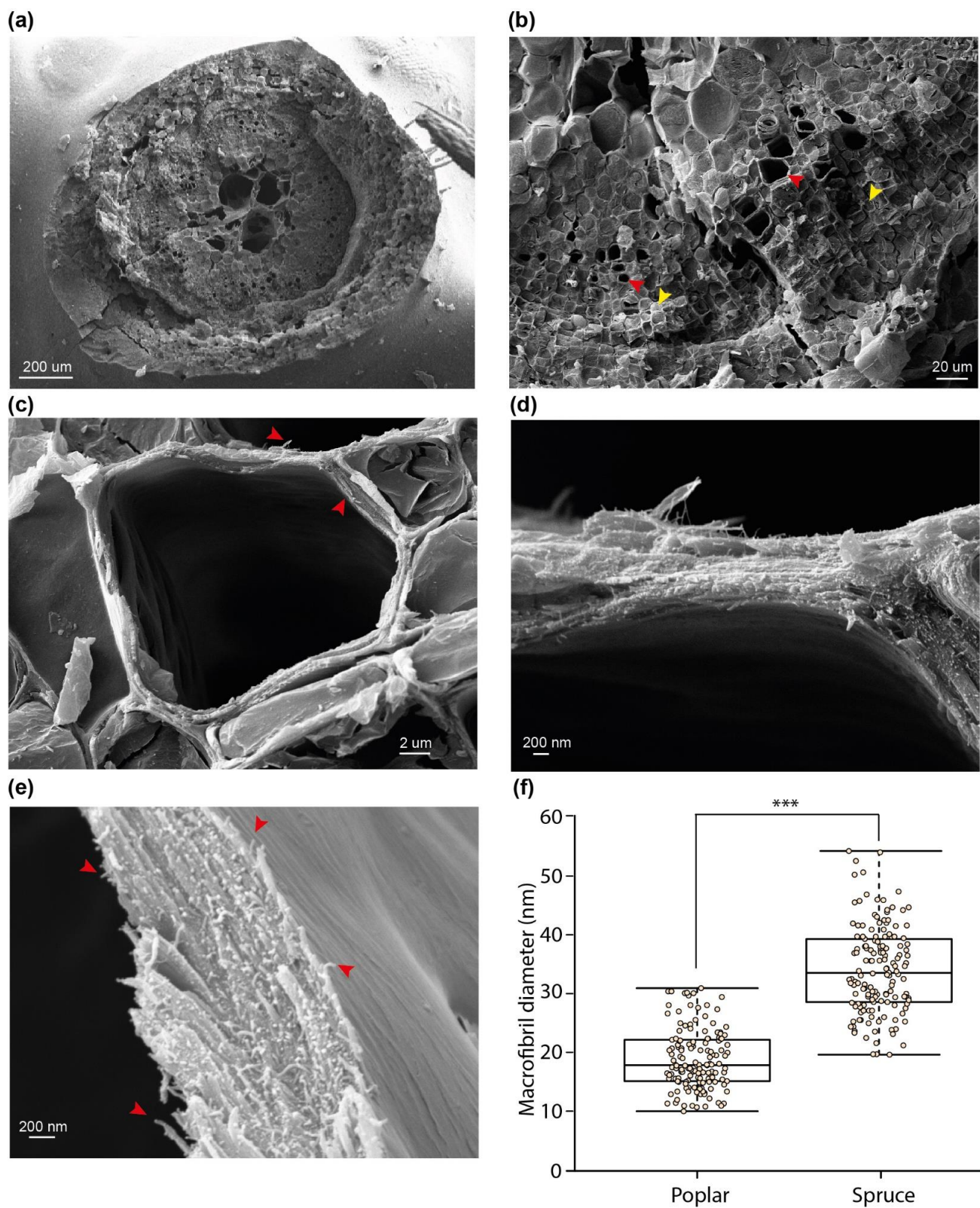
Figure 3

791

792

Cell wall macrofibrils are composed of cellulose, xylan and lignin

794   Figure 4

(a) *irx9*

(b) *irx10*

(c) *esk1*

(d) *4cl1*

(e) *lac4*

(f) *csla2/3/9*

(g)
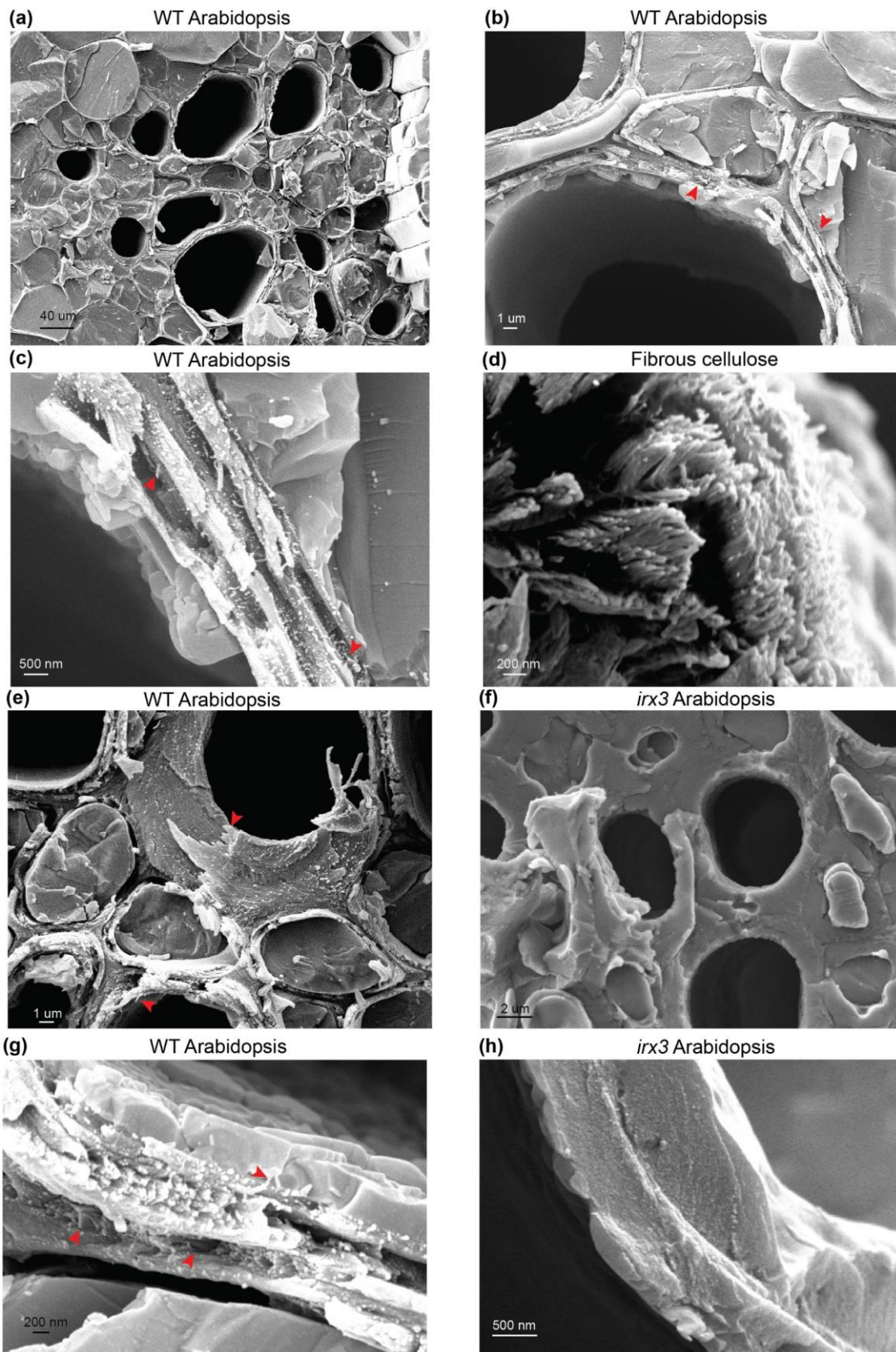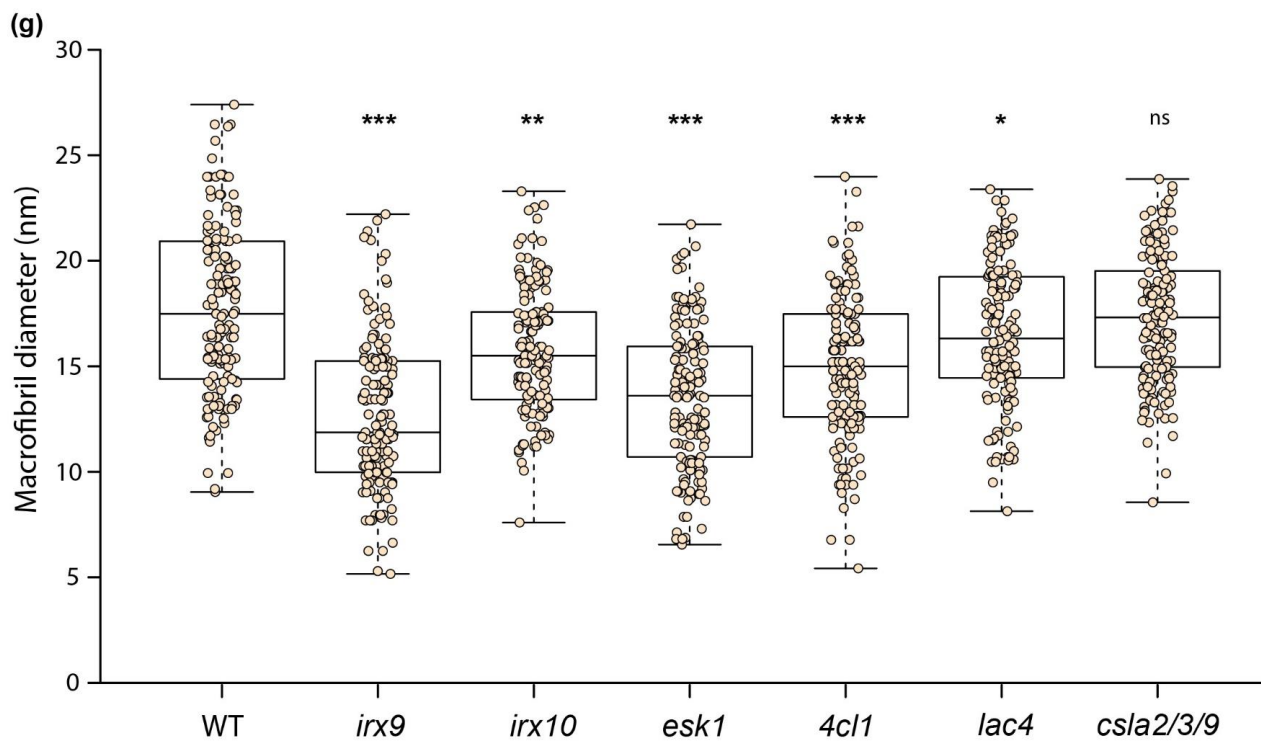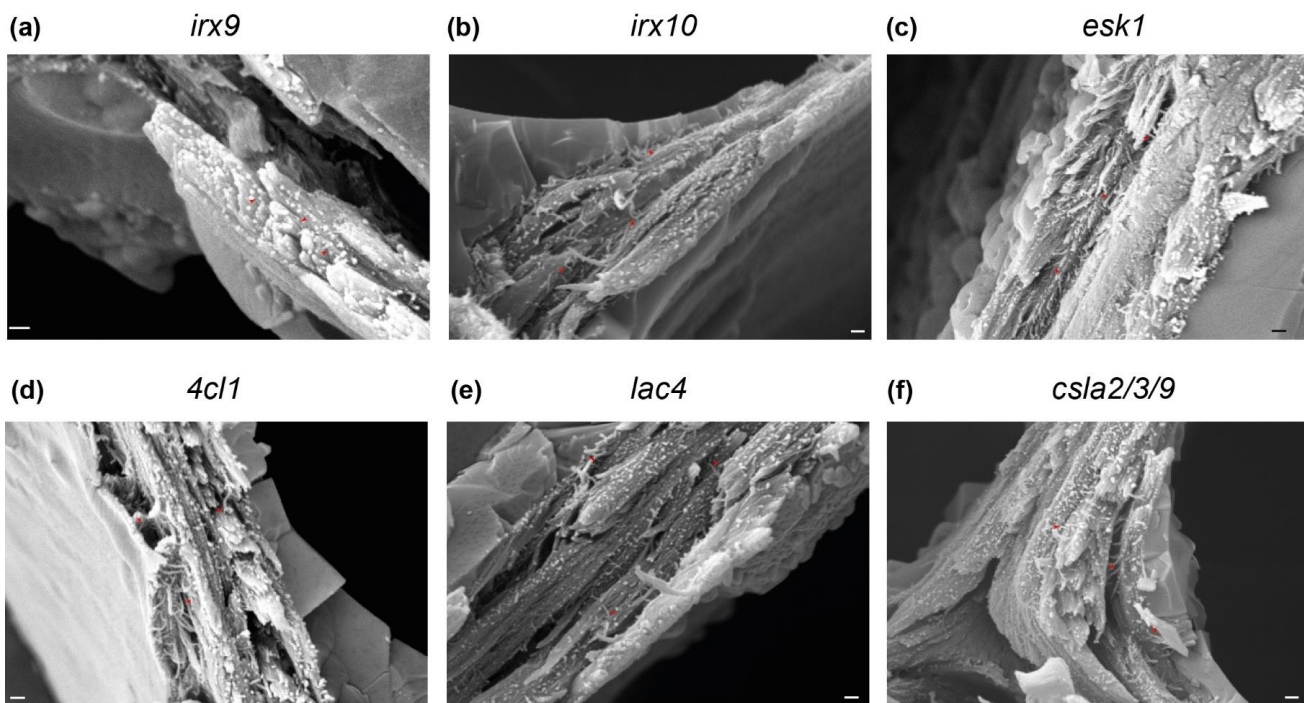
	WT	*irx9*	*irx10*	*esk1*	*4cl1*	*lac4*	*csla2/3/9*
Median macrofibril diameter (nm)	17.5	11.9	15.5	13.6	15.0	16.3	17.3

795

796

797   Figure 5

798

799